JACS
JOURNAL OF THE AMERICAN CHEMICAL SOCIETY

Article

pubs.acs.org/JACS

Fluorescence-Quenched Substrates for Live Cell Imaging of Human Glucocerebrosidase Activity

Anuj K. Yadav,[†] David L. Shen,[†,§] Xiaoyang Shan,[†] Xu He,[‡] Allison R. Kermode,[‡] and David J. Vocadlo*[,†,§]

[†]Department of Chemistry, [‡]Department of Biological Sciences, and [§]Department of Molecular Biology and Biochemistry, Simon Fraser University, Burnaby, British Columbia V5A 1S6, Canada

Supporting Information

ABSTRACT: Deficiency of the lysosomal glycoside hydrolase glucocerebrosidase (GCase) leads to abnormal accumulation of glucosyl ceramide in lysosomes and the development of the lysosomal storage disease known as Gaucher's disease. More recently, mutations in the *GBA1* gene that encodes GCase have been uncovered as a major genetic risk factor for Parkinson's disease (PD). Current therapeutic strategies to increase GCase activity in lysosomes involve enzyme replacement therapy (ERT) and molecular chaperone therapy. One challenge associated with developing and optimizing these therapies is the difficulty in determining levels of GCase activity present within the lysosomes of live cells. Indeed, visualizing the activity of endogenous levels of any glycoside hydrolases, including GCase, has proven problematic within live mammalian cells. Here we describe the successful modular design and synthesis of fluorescence-quenched substrates for GCase. The selection of a suitable fluorophore and quencher pair permits the generation of substrates that allow convenient time-dependent monitoring of endogenous GCase activity within cells as well as localization of activity within lysosomes. These efficiently quenched (~99.9%) fluorescent substrates also permit assessment of GCase inhibition in live cells by either confocal microscopy or high content imaging. Such substrates should enable improved understanding of GCase in situ as well the optimization of small-molecule chaperones for this enzyme. These findings also suggest routes to generate fluorescence-quenched substrates for other mammalian glycoside hydrolases for use in live cell imaging.

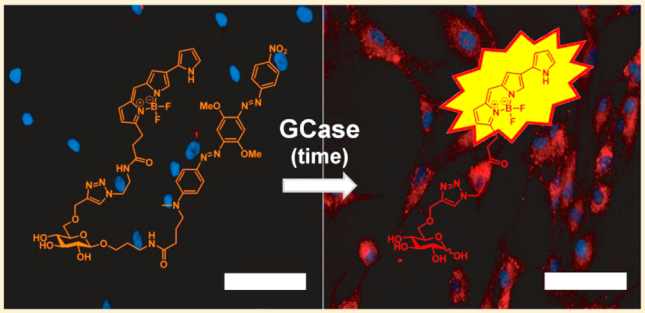

INTRODUCTION

Acid β-glucosidase (GCase) is a lysosomal lipid hydrolase, a membrane-associated glycoprotein that cleaves glucosylceramide (GlcCer) into glucose and ceramide.[1] GCase is a member of CAZy glycoside hydrolase family GH30 (for a description of the CAZy classification system, see www.cazy.org and ref 1). Homozygous loss-of-function mutations[2,3] in the gene encoding GCase (*GBA1*) cause Gaucher's disease (GD), a lysosomal storage disorder with a recessive pattern of inheritance. There are more than 280 known mutations, though the variation in disease penetrance is widely heterogeneous even among identical twins.[4] Most of these mutations lead to single amino acid changes, and the resulting mutant enzymes typically have some residual activity. The resulting decreased GCase activity within humans causes the detrimental accumulation of glucosylceramide within the lysosomes of affected tissues, which is what drives GD and is a key pathological feature of this illness. GD has been classified into three types.[5] Non-neuronopathic (type 1 GD) is the most common of these types, affecting 1 in 10 000 within the general population. Neuronopathic GD includes types 2 and 3, both of which are fatal. Type 2 is more severe than type 3, exhibiting central nervous system (CNS) involvement that manifests within a year of birth. Type 3 GD is milder and manifests later in life but still usually leads to death by the age of 30.

Two different types of treatments have been introduced for type 1 GD. One is enzyme replacement therapy (ERT),[6] which is based on chronic intravenous administration of recombinant GCase. The other is substrate reduction therapy (SRT),[7] which is based on chronic oral administration of an inhibitor of glucosylceramide synthase, which is the enzyme catalyzing the formation of glucosylceramide. Over the past decade an alternative experimental approach called chaperone therapy has gained increasing attention.[8,9]

Most mutations in the *GBA1* gene lead to expression of unstable mutant forms of GCase, which do not reach the lysosome and instead undergo endoplasmic reticulum-associated degradation (ERAD). As a result, levels of active GCase within lysosomes are diminished in those individuals carrying such mutant *GBA1* alleles. However, small-molecule ligands of GCase that are inhibitors have been shown to serve as chaperones that can stabilize mutant GCase, helping it to pass quality control and reach lysosomes. After diffusion of the

Received: October 22, 2014
Published: January 5, 2015

DOI: 10.1021/ja5106738
J. Am. Chem. Soc. 2015, 137, 1181−1189

inhibitor out of the cell, chaperoned mutant GCase within lysosomes is stable and functional. A benefit of this approach is that, unlike recombinant enzyme delivered intravenously, such small-molecule chaperones are brain-penetrant and might therefore be of benefit in neuronopathic Gaucher's disease.

Mutations in *GBA1* have also been implicated in Lewy body diseases (LBDs) such as Parkinson's disease (PD).[10−12] Unexpectedly, mutations in *GBA1* have emerged in the past few years as a major genetic risk factor for PD[13−15] and have been shown to exacerbate the progression of disease.[14,16] Furthermore, PD patients, regardless of whether they carry mutations in GCase, appear to have lower GCase activity in the central nervous system.[17,18] Recent data in which transgenic overexpression of GCase in a PD mouse model reduced Lewy body pathology have suggested that loss of function of GCase contributes to α-synuclein toxicity.[19,20] Accordingly, there is great interest in developing approaches, including chaperone therapy,[21] to enhance the activity of GCase within cells, since this may enable the development of a disease-modifying therapy for both GD and PD.

Generally, the efficiency of inhibitory chaperones for GCase is established by monitoring increases in the levels of this enzyme by immunoblotting of cell lysates.[9,22−24] One difficulty within the field, however, is that there are few methods to visualize and quantify the effects of pharmacological chaperones directly in living cells. The need for such a method is notable for GCase because inhibitory chaperones may persist in cells, inhibiting GCase activity within lysosomes despite there being increased GCase present as assessed by immunoblot analyses. Moreover, the ability to visualize the localization of GCase activity following administration of chaperones could help in monitoring trafficking of the active form of this enzyme. Accordingly, there is a need for methods to monitor GCase activity in live cells.

Fluorogenic substrates for GCase have been described and used to quantify GCase activity,[25,26] but these have not proven useful for direct monitoring of active enzyme by live cell imaging. Recently, Overkleeft and co-workers described an elegant approach[27] using activity-based probes (ABPs) to monitor total levels of active GCase enzyme in cell lysates and even to image functional GCase within fixed cells. Though exquisitely sensitive, one limitation to using such covalent inactivators to monitor GCase activity is that these probes lead to complete inactivation of GCase over time, even in the presence of enzyme modulators including competitive inhibitors. Therefore, inspired by the studies by Overkleeft and co-workers on inactivators of GCase, we set out to design a fluorescence-quenched substrate that would enable us to monitor not the total level of GCase in cells but rather the amount of GCase activity present within live cells. Such substrates could therefore prove to be valuable for monitoring the in situ activity of GCase directly within cells in the presence of modulators. Though fluorogenic substrates exist to monitor abundantly expressed marker glycosidases such as *Escherichia coli* and scenescence-associated β-galactosidase,[28−31] to the best of our knowledge, no substrate has been developed for mammalian glycoside hydrolases that enables quantitative imaging of normal endogenous levels of enzymatic activity within live mammalian cells.

Given that fluorescence-quenched substrates of proteases are proving to be powerful tools to study their function in live cells,[32−35] we considered various designs for fluorescence-quenched substrates for GCase. However, the design of fluorescence-quenched, or fluorescence resonance energy transfer (FRET)-based, glycoside hydrolase probes is more problematic than for proteases and is lagging behind. This difficulty in creating such substrates for glycoside hydrolases stems from the pocket-shaped topology of the active site of *exo*-glycoside hydrolases as compared to the cleftlike architecture found for proteases. The constrained active-site architecture therefore makes it difficult to design glycoside hydrolase substrates in which such groups are appropriately positioned.

Though the topic of fluorescence-quenched substrates for glycoside hydrolases is gaining attention, current efforts have not proven useful for monitoring the endogenous activity of any glycoside hydrolase in mammalian cells. Furthermore, initial efforts have yielded probes that can also inactivate the enzyme of interest due to formation of a transient reactive quinine methide intermediate within the enzyme active site.[36,37] Accordingly, we felt that a fluorescence-quenched GCase substrate, which would enable the enzyme to turn over multiple molecules, could prove generally useful to assess the enzymatic activity of GCase within live cells. Here we describe the design and synthesis of an efficiently quenched fluorescent GCase substrate that enables localization and quantification of enzyme activity in live human cells by imaging.

RESULTS AND DISCUSSION

Synthesis and in Vitro Evaluation of Quenched Substrate-Based Probes. For live cell monitoring of GCase activity, an important criterion is that the probe should be able to gain access to the lysosomes and have a low background fluorescence. We therefore set out to design an efficiently quenched fluorescent substrate that has a basic functionality that would favor lysosomal uptake, as well as a reasonable balance of hydrophilicity and polar functional groups that could facilitate uptake of substrate by cells.

To satisfy these criteria, we developed a modular synthesis that could accommodate the installation of different fluorophore−quencher pairs. We noted that GCase accommodates the long aliphatic chain of the ceramide moiety of GlcCer, the natural substrate of GCase, which is pendent to the anomeric center. We therefore chose to attach the quencher group to this center, using an aliphatic spacer to avoid steric congestion close to the active site, with the expectation that this linker and the hydrophobic quencher would be tolerated by the enzyme. Furthermore, it has been observed that modification to the 6-position of glucose can be tolerated by GCase.[27] We therefore speculated that installation of a fluorophore at this position within the substrate might be tolerated by the enzyme. By positioning the quencher−fluorophore pair at these sites to place them in close proximity to each other, we also anticipated that highly efficient quenching could take place through both contact quenching and FRET. Furthermore, by appending the fluorophore, as opposed to the quencher, to the 6-position of the glucopyranose ring, we anticipated that diffusion of the fluorophore out of the lysosome would be hindered by the highly polar pendent sugar ring (Figure 1).

The probe was assembled through the use of bifunctionalized intermediate **7** (Scheme 1). To obtain this intermediate, we carried out $BF_3{\cdot}Et_2O$-promoted glycosylation of penta-*O*-acetyl β-D-glucopyranose **3** with 3-bromopropanol, followed by displacement of the bromide with sodium azide to afford glycoside **4**.[38,39] Deacetylation, followed by regioselective propargylation of the 6-hydroxyl using sodium hydride, then followed by triphenylphosphine reduction of the azide

DOI: 10.1021/ja5106738
J. Am. Chem. Soc. 2015, 137, 1181−1189

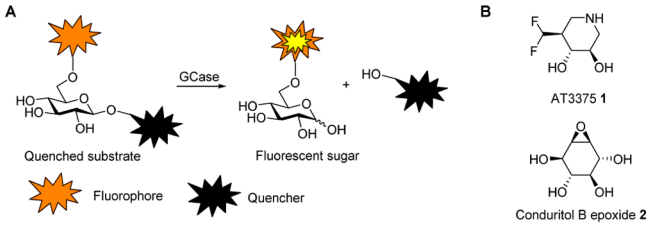

Figure 1. Design of fluorescence-quenched GCase substrate and known GCase inhibitors used in this study. (A) General reaction scheme showing the design for fluorescence-quenched GCase substrates. (B) Proposed structure of GCase inhibitory chaperone AT3375 **1** and the structure of inactivator conduritol B epoxide (CBE) **2**.

Scheme 1. Synthesis of Amine Intermediate 7[a]

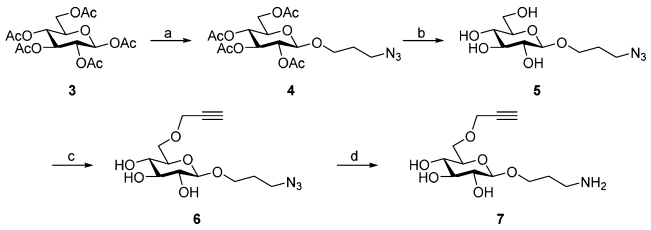

[a](a) (i) 3-Br-propanol, $BF_3{\cdot}Et_2O$, 60%; (ii) NaN_3, DMF, 80 °C; 70%. (b) Cat. K_2CO_3, MeOH, quantitative. (c) NaH, propargyl bromide, 0 °C, 40%. (d) TPP, Et_2O, H_2O, 60%.

functionality, led to the desired intermediate **7**. Using this intermediate **7**, we first tested the potential of this substrate design using the readily available building blocks EDANS, 5-[(2-azidoethyl)amino]naphthalene-1-sulfonic acid, as the fluorophore and DABCYL, 4-{[4-(dimethylamino)phenyl]azo}-benzoic acid, as the quencher. The succinimidyl ester (DABCYL-NHS) was used to acylate the amine of intermediate **7** to obtain propargyl-functionalized **8a**. Cu(I)-catalyzed coupling of the propargyl group with EDANS azide afforded the desired first-generation substrate **9a** (Scheme 2).

With substrate **9a** in hand, we evaluated its quenching efficiency. The intact substrate shows strikingly little fluorescence, whereas the chemically synthesized cleaved substrate shows much greater fluorescence with a spectrum matching that of the free fluorophore (excitation max = 338 nm and emission max = 490 nm; Figure S3, Supporting Information). We calculated that quenching is 97.6% efficient for this substrate at the concentrations used for in vitro assays (Figure S5, Supporting Information), which supports this probe design being effective for dark-to-light switching. We next evaluated the processing of this substrate by GCase in vitro. Because probe **9a** shows limited solubility, we were unable to assess activity at concentrations higher than 200 μM, precluding the determination of a K_m value. Because K_m is a composite rate constant, we assayed substrate **9a** as a competitive inhibitor of GCase in order to determine whether it might bind more tightly to the enzyme than the K_m suggests. We find no sign of saturation of the enzyme up to 100 μM (data not shown), which is consistent with the Michaelis–Menten analysis described just above. Nevertheless, we were able to establish the second-order rate constant for cleavage of this substrate, $k_{cat}/K_m = 60 \pm 2$ $min^{-1}{\cdot}mM^{-1}$, which is 2.9-fold poorer than that of the widely used GCase substrate 4-methylumbelliferyl β-D-glucopyranoside (4-MUGlc), $k_{cat}/K_m = 176 \pm 2$ $min^{-1}{\cdot}mM^{-1}$ (Figure S7, Supporting Information).

Scheme 2. Synthesis of Fluorescent Quenched Substrates 9a and 9b[a]

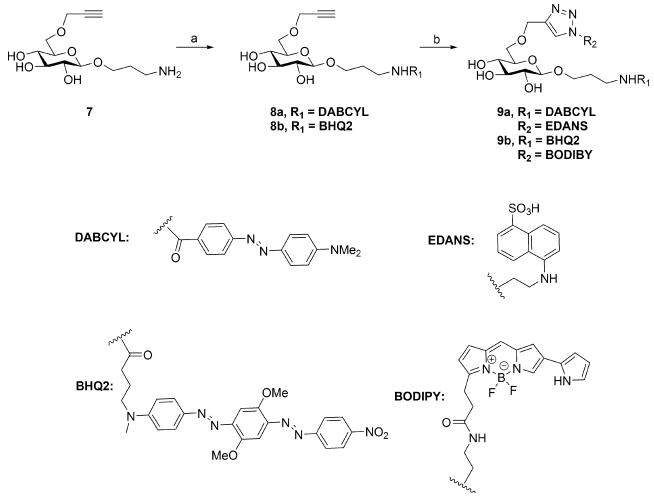

[a]For **8a**: (a) DABCYL-NHS, DIPEA, DMF, quantitative. For **8b**: (a) BHQ2-NHS, DIPEA, DMF, quantitative. For **9a**: (b) EDANS-N_3, NaAsc., $CuSO_4$, DCM/H_2O (1:1), 50%. For **9b**: (b) (i) $N_3CH_2CH_2NHBoc$, sodium ascorbate, $CuSO_4$, DCM/H_2O (1:1), 50%; (ii) 90% TFA in DCM at 0°C, quantitative; (iii) BODIPY-NHS, DIPEA, DMF, 80%.

With the realization that this probe design is suitable for generating fluorescence-quenched GCase substrates, we next set out to develop a second-generation probe that could be used for live cell imaging. Because probe **9a** fluoresces with an emission maximum at 490 nm, we found it incompatible for use in live cell imaging due to endogenous cellular fluorescence at this wavelength. We therefore turned to using boron–dipyrromethene (BODIPY) 576/589, which would enable using a more red-shifted laser that would limit damage to cells during imaging as well as reducing autofluorescence from cells. We selected Black Hole Quencher 2 (BHQ2) as the quencher because its absorption band overlaps effectively with the emission band of BODIPY 576/589, suggesting FRET-based quenching should be efficient. Moreover, we reasoned that the mildly basic aniline within the substrate would favor its accumulation within the acidic environment of lysosomes. The BHQ2 carboxylic acid succinimidyl ester (BHQ2-NHS) quencher was therefore first coupled to the amine by an amide coupling reaction to afford **8b**.

To keep the sugar scaffold the same as in substrate **9a**, we first attached a $BocNHCH_2CH_2N_3$ linker.[40] Copper(I) catalyzed azide–alkyne cycloaddition reaction (CuAAC) with $BocNHCH_2CH_2N_3$ yielded the terminal Boc-protected amine. After removal of the *tert*-butyloxycarbonyl (Boc) protecting group, the resulting amine intermediate was reacted with the *N*-hydroxysuccinimide ester of BODIPY 576/589 (BODIPY-NHS) to furnish the second-generation substrate **9b** (Scheme 2). We found the excitation and emission maxima for **9b** were 574 and 595 nm, respectively (Figure S4, Supporting Information). Notably, substrate **9b** showed 99.9% quenching efficiency (Figure S6, Supporting Information) and was processed in vitro by GCase (Figure S8, Supporting Information) 2.2-fold worse than substrate **9a**.

Live Cell Imaging of GCase Activity in Human Fibroblasts. With probe **9b** in hand, we evaluated whether time- and dose-dependent processing of substrate could be

DOI: 10.1021/ja5106738
J. Am. Chem. Soc. 2015, 137, 1181–1189

observed in human primary skin fibroblasts. High content imaging of cells treated with 4′,6-diamidino-2-phenylindole (DAPI), to stain nuclei, and 5 μM substrate **9b** revealed increasing fluorescence as a function of time (Figure 2A). The

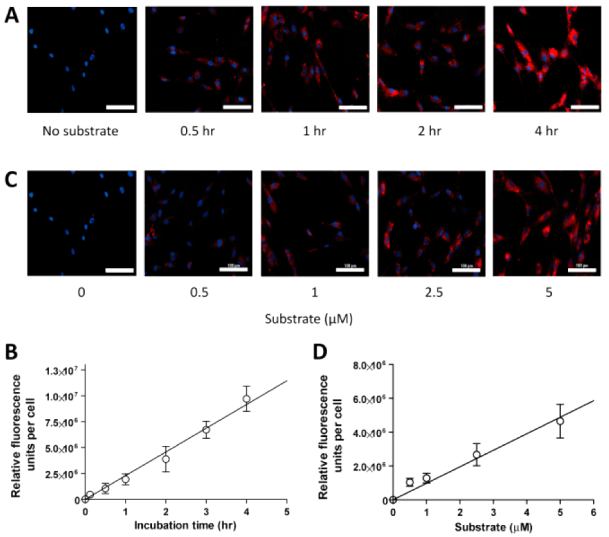

Figure 2. Time- and dose-dependent increases in fluorescence upon incubation of GCase fluorescence-quenched substrate **9b** with human fibroblasts. (A) Representative images showing that incubation with substrate **9b** (5 μM) leads to time-dependent increases in fluorescence observed within primary human fibroblasts. (B) Quantitative relative fluorescence intensity per cell at various time points to 4 h reveals a linear increase in signal as a function of time. (C) Representative images showing that fluorescence intensity within human fibroblasts, observed after 2 h of incubation with fluorescence-quenched probe **9b**, increases with increasing probe concentration. (D) Quantitative relative fluorescence intensity per cell at various concentrations of fluorescence-quenched substrate **9b** reveals a linear increase in fluorescence as a function of probe concentration. The blue signal in panels A and C represents staining of nuclei with DAPI, and the red signal represents the cleaved product of **9b**. White scale bars represent 100 μm. Error bars represent the standard error of the mean obtained from four randomly selected fields from two independent experiments.

fluorescence associated with cleavage of probe **9b** was present in a punctate pattern consistent with a lysosomal distribution. By integrating the fluorescence intensity from randomly selected fields, we observed a quantitative increase in fluorescence as a function of time (Figure 2B). We next examined the dose-dependent cellular fluorescence of probe **9b** (Figure 2C) and observed a linear increase in fluorescence that depended on the concentration of **9b** (Figure 2D). As assessed by the trypan blue assay, we observed no toxicity associated with the probe upon incubating cells for 3−20 h (data not shown). While these data reveal probe **9b** is processed in cells to result in the fluorescent product, we sought to test whether the observed fluorescence was dependent on GCase activity.

To assess whether the punctuate fluorescence observed is distributed in lysosomes, we carried out colocalization experiments using LysoTracker Green DND-26, which is a widely used lysosomal marker compatible with live cell imaging. We therefore treated cells with substrate **9b** for 3 h, after which LysoTracker Green was added to the culture for 15 min before imaging by confocal microscopy. We observed extensive superposition of substrate **9b**-associated fluorescence and LysoTracker Green fluorescence (Figure 3), indicating that

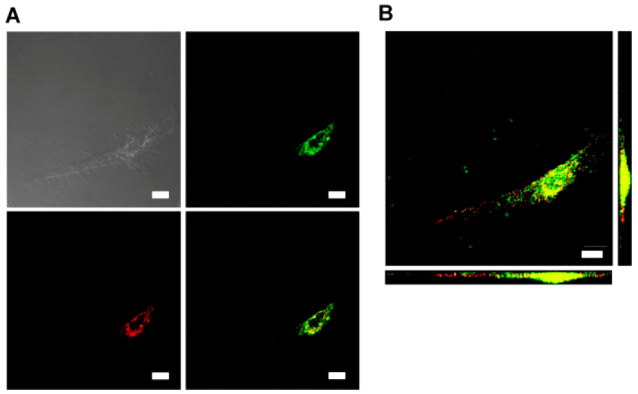

Figure 3. Processing of fluorescence-quenched substrate **9b** in lysosomes. (A) Fluorescence images are from one *Z*-section selected from the center of the stack. (Upper left) Differential interference contrast (DIC) image; (upper right) fluorescence image (green) for LysoTracker Green; (lower left) fluorescence image (red) for signal from processed substrate **9b**; (bottom right) merged image. (B) Representative image showing the maximum intensity projection of *Z*-sections with the vertical slice representing the *yz*-axis and the horizontal slice representing the *xz*-axis. Scale bars represent 20 μm.

the fluorescence associated with cleavage of **9b** occurs in the lysosomal compartments of the cells. Analysis of the *Z*-direction stack also indicated substrate processing was occurring within lysosomes (Figure 3B).

Within human cells there are three β-glucosidases, including GBA2[21] from family GH116 and GBA3[22] from family GH1, which respectively have membrane and cytosolic localizations. Those enzymes can be distinguished from GCase on the basis of their localization but also because they are relatively insensitive to conduritol B epoxide (CBE), whereas lysosomal GCase is quickly inactivated by CBE.[27,43,44] Therefore, to explore the in-cell specificity of substrate **9b** toward GCase, we incubated cells with CBE or vehicle alone for 16 h, then treated the cells with both substrate **9b** and DAPI for 2 h. We then imaged cells by high content imaging (Figure 4) as a function of cell concentration. The analysis of different cell densities indicates the high content imaging assay does not show significant variability as a function of the number of cells plated within the range used here. We found that CBE-treated cells showed little fluorescence as compared to vehicle-treated control cells (Figure 4). We also evaluated substrate **9b** in a human neuronal cell culture model, SK-N-SH neuroblastoma cells, and found that this substrate was processed within these cells in a similar manner (Figure S9, Supporting Information), indicating that such substrates should prove useful in various cell types. These data indicate that probe **9b** is predominantly processed by GCase within cells, supporting its use as a tool to image GCase activity within live cells across a range of cell densities.

Finally, to assess whether substrate **9b** can be used to quantify chaperoning of wild-type GCase, we used the inhibitory GCase chaperone AT3375, for which the proposed structure is shown in Figure 1.[45] We treated cells with AT3375 as has been previously described for isofagomine[26] to induce chaperoning of wild-type GCase. Treating cells for 5 days with AT3375, washing cells overnight with fresh medium, and then incubating with substrate **9b** for 3 h resulted in a 1.4-fold increase in processing of substrate **9b** as observed by fluorescence microscopy (Figure 5). This increase in cleavage of substrate **9b** is consistent with previous results for use of

DOI: 10.1021/ja5106738
J. Am. Chem. Soc. 2015, 137, 1181−1189

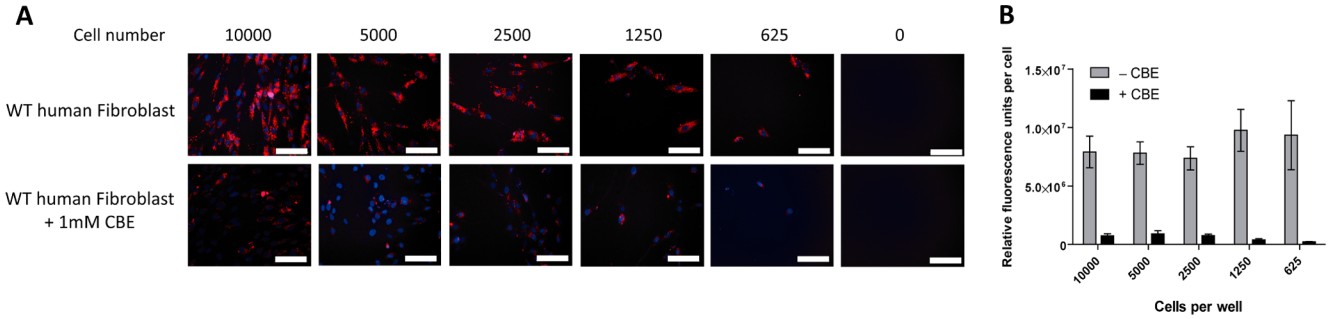

Figure 4. GCase-dependent processing of fluorescence-quenched substrate **9b**. (A) Representative images showing that treatment of fibroblasts with CBE (**2**) leads to decreased fluorescence associated with processing of fluorescence-quenched substrate **9b** within human fibroblasts. The upper line of images in panel A are fluorescence images obtained in the absence of CBE, and the bottom row are fluorescence images obtained in the presence of CBE. (B) Quantitative relative fluorescence intensity per cell for cells treated with substrate **9b** and substrate **9b** plus CBE at different concentrations of cells in each well. White scale bars represent 100 μm.

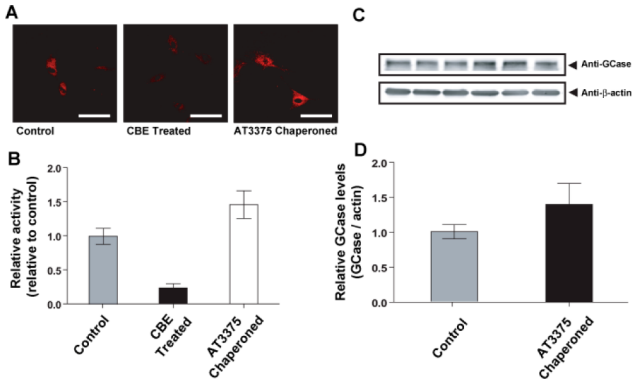

Figure 5. Incubation of fibroblasts with the chemical chaperone AT3375 (10 μM) for 5 days, followed by 1 day washout, results in increased GCase activity and protein. (A) Representative images showing that chaperoning with AT3375 leads to increased GCase activity relative to control, as reflected in the extent of turnover of substrate **9b** (5 μM). CBE treatment reduces GCase activity. (B) Quantitative relative fluorescence intensity per cell for cells treated with substrate **9b**, substrate **9b** plus CBE, and AT3375 for 5 days followed by washout for 1 day. (C) Immunoblot analysis shows that chaperoning with AT3375 for 5 days leads to an increase in GCase protein levels. (D) Quantitative relative immunoreactivity for GCase levels in cells treated with AT3375 or vehicle alone as assessed by immunoblot. Scale bars represent 50 μm.

isofagomine to chaperone GCase[26] in human fibroblasts. Furthermore, we found by immunoblot assay that the levels of GCase protein were increased upon chaperoning by AT3375 to the same extent as measured by substrate **9b** (Figure 5). These data show that live cell imaging with substrate **9b** can be used to monitor GCase activity in live cells and can be used to quantitatively assess chaperoning of GCase.

CONCLUSIONS

Collectively, these studies reveal a convenient modular design for generation of fluorescence-quenched substrates for GCase. These substrates are very efficiently quenched when intact but give rise to fluorescence when hydrolytically cleaved by GCase. Substrate **9b** shows greater than 99.9% quenching efficiency, which enables direct visualization of GCase activity in live cells. Given increasing interest in the physiological and pathophysiological roles of GCase in both Gaucher's and Parkinson's diseases as well as the characterization of inhibitors and chaperones of GCase, we anticipate that substrate **9b** and analogues may find common use for those interested in identifying GCase chaperones as well as for studying the trafficking and regulation of GCase within cells. Additionally, the compatibility of this approach with high content imaging in live cells opens the door to screening for endogenous protein modifiers of GCase activity as well as screening for activators that function within cells to influence GCase activity.

The use of common orthogonally functionalized intermediate **7** within the synthesis also enables late installation of the fluorophore and quencher. This flexibility opens the door to further optimization of such GCase substrates. Through the judicious selection of fluorophores in combination with various imaging systems, it may be feasible to perform super-resolution imaging of GCase activity or imaging of GCase within animal models. More generally, to the best of our knowledge, direct quantitative imaging of mammalian glycoside hydrolases at normal endogenous levels has not been previously demonstrated within live cells. Accordingly, this strategy of using fluorescence-quenched substrates may find, by adaptation, application for the investigation of other mammalian glycoside hydrolases.

EXPERIMENTAL SECTION

General Information. ^{1}H and ^{13}C NMR spectra were obtained on Bruker AVII 600 (600 MHz for ^{1}H and 151 MHz for ^{13}C) and Bruker AVIII 400 (400 MHz for ^{1}H and 101 MHz for ^{13}C) spectrometers. Unless stated otherwise, deuterated methanol (CD_3OD) was used as the solvent, with CH_3OH (δH 3.31) or CD_3OD (δC 49.00) being employed as internal standards. Mass spectra were recorded on an Agilent 6210 time-of-flight (TOF) liquid chromatography/mass spectrometry (LC/MS) system. The LC system used was an Agilent 1200 HPLC, and the MS was a 6210 high-resolution TOF MS. A Bruker maXis impact quadrupole TOF LC/MS system was also used. This system consists of an Agilent 1200 HPLC and a Bruker maXis impact ultra-high resolution tandem TOF MS. The ionization mode used was positive electrospray ionization (+ESI). Flash chromatography was performed on BDH silica gel or Geduran silica gel 60 with the specified solvents. Thin-layer chromatography (TLC) was performed on Merck silica gel 60 F254 aluminum-backed plates that were stained by heating (≥200 °C) with 5% sulfuric acid in EtOH. Percentage yields for chemical reactions are quoted only for those compounds that were purified by recrystallization or by column chromatography and for which the purity was assessed and verified by ^{1}H NMR spectroscopy. Chemicals and solvents were obtained from Sigma–Aldrich and used without further purification unless otherwise noted. EDANS and DABCYL-NHS ester were purchased from AnaSpec. Inc.; BHQ2 was obtained from Biosearch Technologies; and BODIPY576/589, LysoTracker Green DND-26, and α-minimum

DOI: 10.1021/ja5106738
J. Am. Chem. Soc. 2015, 137, 1181–1189

essential medium (α-MEM, without nucleosides) were from Life Technologies. Liquid chromatography was performed on an Agilent 1100 series HPLC equipped with a C18 column.

Synthetic Procedures for Chemical Compounds. *3-Azidopropyl β-D-Glucopyranoside (**5**).* Anhydrous potassium carbonate (64 mg; 0.46 mmol) was added to a solution of **4** (2.00 g; 4.64 mmol) in MeOH (25 mL). The reaction mixture was stirred overnight at room temperature. TLC: R_f 0.2 in 15% MeOH in $CHCl_3$. After the reaction was juged complete by TLC, the mixture was concentrated and **5** was purified by silica gel column chromatography and eluted with 12% MeOH in $CHCl_3$ to give a viscous liquid: yield 95%, 1.2 g. High-resolution mass spectrometry (HRMS) $[M + Na]^+$ calcd 286.10096, found 286.10090. ^{1}H NMR (600 MHz, MeOD) δ 1.87 (p, J = 6.5 Hz, 2H), 3.17 (dd, J = 9.1, 7.9 Hz, 1H), 3.29−3.24 (m, 2H), 3.35 (m, 1H) 3.45 (t, J = 6.6 Hz, 2H), 3.65 (ddd, J = 12.3, 11.1, 5.7 Hz, 2H), 3.88−3.83 (m, 1H), 3.97 (dt, J = 10.1, 6.0 Hz, 1H), 4.25 (d, J = 7.8 Hz, 1H). ^{13}C NMR (151 MHz, MeOD) δ 104.45, 78.07, 77.95, 75.11, 71.65, 67.57, 62.76, 49.43, 30.26.

*3-Azidopropyl-6-O-propargyl β-D-Glucopyranoside (**6**).* To a solution of **5** (193 mg, 0.73 mmol) in anhydrous *N*,*N*-dimethylformamide (DMF, 5 mL) at 0 °C was added a 60% dispersion of NaH (132 mg; 3.30 mmol) in mineral oil, and the mixture was stirred for 5 min. Propargyl bromide (109 mg, 0.73 mmol) was then added dropwise to the mixture, and stirring was continued for 30 min. TLC: R_f 0.3 in 10% MeOH in $CHCl_3$. After the reaction was judged complete, water was added and the mixture was extracted with ethyl acetate, dried over Na_2SO_4, and concentrated. Compound **6** was purified by silica gel column chromatography and eluted with 5% MeOH in $CHCl_3$: yield 40%, 88 mg. HRMS $[M + H]^+$ calcd 302.13466, found 302.13386. ^{1}H NMR (600 MHz, MeOD) δ 1.92−1.81 (m, 2H), 2.84 (t, J = 2.4 Hz, 1H), 3.20−3.14 (m, 1H), 3.30−3.26 (m, 1H), 3.34 (d, J = 7.9 Hz, 1H), 3.42−3.37 (m, 1H), 3.45 (t, J = 5.1 Hz, 2H), 3.70−3.60 (m, 2H), 3.95−3.85 (m, 2H), 4.27−4.17 (m, 3H). ^{13}C NMR (151 MHz, MeOD) δ 102.50, 78.60, 76.02, 74.80, 73.91, 73.02, 69.64, 68.30, 65.72, 57.46, 28.31.

*3-Amido-DABCYL-6-O-propargyl β-D-Glucopyranoside (**8a**).* To a mixture of anhydrous diethyl ether (3 mL) containing anhydrous tetrahydrofuran (THF, 1 mL) and **6** (40 mg; 0.13 mmol) was added triphenylphosphine (TPP) (87 mg, 0.32 mmol). The reaction mixture was stirred at room temperature for 3 h, after which H_2O (0.3 mL) was added and the mixture was allowed to stir overnight. TLC: R_f 0.2 in EtOAc/MeOH/H_2O (3:2:1). The reaction mixture was concentrated after being judged complete by TLC and then resuspended in water and extracted with $CHCl_3$ (3×). The aqueous layer was concentrated and loaded on a short column of silica gel, and the desired intermediate was eluted with EtOAc/MeOH/H_2O (3:2:1) containing 4% aqueous ammonia to furnish crude amine (**7**). This crude amine was used immediately without further purification. HRMS $[M + H]^+$ calcd 276.14416, found 276.14376.

To this crude amine **7** (48 mg, 0.174 mmol) in anhydrous DMF (1 mL) was added DABCYL-NHS (70 mg, 0.192 mmol) and *N*,*N*-diisopropylethylamine (DIPEA, 30 μL, 0.17 mmol). The reaction mixture was stirred overnight at room temperature in the dark. TLC: R_f 0.5 in 10% MeOH in $CHCl_3$. After being judged complete by TLC, the mixture was concentrated and **8a** was purified by silica gel column chromatography and eluted with 5% MeOH in $CHCl_3$: yield 90%, 83 mg. HRMS $[M + H]^+$ calcd: 527.25003, found 527.25021. ^{1}H NMR (400 MHz, MeOD) δ 2.00−1.89 (m, 2H), 2.82 (q, J = 2.8 Hz, 1H), 3.11 (s, 6H), 3.21 (dd, J = 9.0, 7.9 Hz, 1H), 3.37−3.33 (m, 1H), 3.47−3.39 (m, 1H), 3.59−3.52 (m, 2H), 3.76−3.63 (m, 2H), 3.90−3.84 (m, 1H), 3.99 (dt, J = 10.0, 5.9 Hz, 1H), 4.17 (dd, J = 4.1, 2.4 Hz, 2H), 4.30 (d, J = 7.8 Hz, 1H), 6.86−6.79 (m, 2H), 7.88−7.81 (m, 4H), 7.97−7.91 (m, 2H). ^{13}C NMR (101 MHz, MeOD) δ 169.61, 156.38, 154.65, 144.84, 135.95, 129.28, 126.39, 122.97, 112.62, 104.55, 80.54, 78.02, 76.74, 75.99, 75.11, 71.64, 70.28, 68.94, 59.40, 40.38, 38.54, 30.39.

*3-Amido-DABCYL-6-methoxytriazol-EDANS β-D-Glucopyranoside (**9a**).* To a mixture of **8a** (40 mg, 0.076 mmol) and EDANS-azide (53 mg, 0.18 mmol) in H_2O/dichloromethane (DCM) (1.5 mL/1.5 mL) were added sodium ascorbate (45 mg; 0.2277 mmol) and $CuSO_4 \cdot 5H_2O$ (28 mg; 0.11 mmol). The mixture was stirred overnight at room temperature in the dark. TLC: R_f 0.1 in 20% MeOH in $CHCl_3$. The reaction mixture was concentrated and the desired material was purified by reverse-phase HPLC. Elution was performed with a gradient of 20−24% acetonitrile (with 0.1% trifluoroacetic acid, TFA) in H_2O (with 0.1% TFA) over 55 min. The fractions collected from 46 to 48 min afforded pure **9a** (Figure S1, Supporting Information): yield 50%, 31 mg. HRMS $[M + H]^+$ calcd 819.31304, found 819.31359. ^{1}H NMR (601 MHz, MeOD) δ 1.92−1.80 (m, 2H), 3.09 (s, 6H), 3.13 (dt, J = 9.2, 6.9 Hz, 1H), 3.20−3.17 (m, 1H), 3.38−3.32 (m, 2H), 3.42 (dt, J = 3.3, 1.6 Hz, 1H), 3.52−3.45 (m, 2H), 3.58 (dd, J = 10.7, 5.4 Hz, 1H), 3.67−3.60 (m, 1H), 3.78−3.70 (m, 3H), 3.87−3.81 (m, 1H), 4.23 (d, J = 7.8 Hz, 1H), 4.57 (s, 2H), 4.66 (d, J = 6.0 Hz, 2H), 6.61 (t, J = 7.5 Hz, 1H), 6.81 (d, J = 9.2 Hz, 2H), 7.36 (dq, J = 16.4, 8.2 Hz, 2H), 7.82−7.77 (m, 3H), 7.84 (d, J = 9.1 Hz, 2H), 7.92 (d, J = 8.5 Hz, 2H), 8.03 (t, J = 8.8 Hz, 1H), 8.13 (t, J = 8.0 Hz, 1H), 8.20 (t, J = 7.1 Hz, 1H). ^{13}C NMR (151 MHz, MeOD) δ 169.49, 156.35, 154.65, 145.79, 144.83, 144.49, 142.13, 131.59, 129.31, 128.39, 126.79, 126.39, 125.78, 125.18, 123.82, 122.90, 117.10, 112.63, 105.26. 104.53, 77.95, 76.92, 75.10, 71.48, 70.49, 69.04, 65.23, 50.24, 44.74, 40.37, 38.63, 30.30.

*3-Amido-BHQ2-6-O-propargyl β-D-Glucopyranoside (**8b**).* To a mixture of **7** (2.5 mg, 0.009 mmol) and BHQ2-NHS (5 mg, 0.008 mmol) in anhydrous DMF (0.6 mL) was added diisopropylethyl amine (1.6 μL, 0.0090 mmol). The reaction mixture was stirred overnight in the dark at room temperature. TLC: R_f 0.5 in 10% MeOH in $CHCl_3$. After completion of the reaction as judged by TLC, the mixture was concentrated and **8b** was purified by silica gel column chromatography and eluted with 8% MeOH in $CHCl_3$: yield 90%, 6.2 mg. Low-resolution MS $[M + H]^+$ calcd 764.3250, found 764.3241. ^{1}H NMR (600 MHz, MeOD) δ 1.80 (t, J = 6.0 Hz, 2H), 1.99−1.92 (m, 2H), 2.29 (t, J = 7.4 Hz, 2H), 2.85 (s, 1H), 3.12 (s, 3H), 3.21−3.15 (m, 1H), 3.54 (t, J = 7.6 Hz, 2H), 3.63 (dd, J = 24.5, 13.2 Hz, 2H), 3.93−3.83 (m, 2H), 4.02 (s, 3H), 4.06 (s, 3H), 4.22 (dd, J = 26.4, 6.1 Hz, 3H), 6.88 (d, J = 9.3 Hz, 2H), 7.49 (s, 1H), 7.55 (s, 1H), 7.90 (d, J = 9.2 Hz, 2H), 8.10 (d, J = 8.6 Hz, 2H), 8.42 (d, J = 11.2 Hz, 2H). ^{13}C NMR (151 MHz, MeOD) δ 173.27, 155.74, 152.99, 151.90, 150.22, 147.99, 146.08, 143.59, 141.40, 125.23, 123.82, 122.66, 110.69, 102.39, 100.25, 99.37, 78.62, 76.03, 74.70, 74.05, 73.06, 69.64, 68.38, 66.58, 57.46, 55.32, 50.66, 47.85, 36.79, 35.76, 31.97, 28.29, 22.16.

*3-Amido-BHQ2-6-methoxytriazolyl-1′-ethyl-3′-amido-BODIPY576/589 β-D-Glucopyranoside (**9b**).* A suspension of **8b** (3 mg; 0.004 mmol) and $N_3CH_2CH_2NHBoc$ in H_2O/DCM (1.5 mL/1.5 mL) was set to stir at room temperature. To this mixture were added sodium ascorbate (2.3 mg, 0.012 mmol) and $CuSO_4 \cdot 5H_2O$ (1.4 mg, 0.0058 mmol), and stirring was continued overnight at room temperature. After the reaction was judged complete by TLC, the mixture was concentrated, filtered through a column of silica gel, and then cooled to 0 °C after which an ice cold solution of 90% TFA in DCM (3 mL) was added and the mixture was stirred for two hours after which it was concentrated. The resulting solution was then directly used for coupling with BODIPY-NHS. For the coupling of this crude intermediate (4.5 mg, 0.0052 mmol), anhydrous DMF (0.8 mL) was added, followed by diisopropylethyl amine (0.9 μL, 0.005 mmol) and BODIPY-NHS (2.4 mg, 0.0057 mmol). The resulting reaction mixture was stirred overnight in the dark. TLC: R_f 0.3 in 10% MeOH in $CHCl_3$. After being judged complete by TLC, the mixture was concentrated and **9b** was purified by silica gel column chromatography and eluted with 7% MeOH in $CHCl_3$. The material was further purified by HPLC (Figure S2, Supporting Information): yield 60%, 2.7 mg. HRMS $[M + H]^+$ calcd 1161.4893, found 1161.4888. ^{1}H NMR (600 MHz, MeOD) δ 1.76 (d, J = 6.3 Hz, 3H), 1.93 (d, J = 7.7 Hz, 2H), 2.23 (d, J = 7.2 Hz, 2H), 2.59−2.55 (m, 2H), 3.07 (s, 3H), 3.16 (t, J = 7.0 Hz, 1H), 3.21 (t, J = 7.7 Hz, 3H), 3.50−3.46 (m, 2H), 3.56 (dd, J = 10.3, 6.1 Hz, 1H), 3.66−3.60 (m, 5H), 3.77 (d, J = 12.8 Hz, 1H), 3.87−3.82 (m, 1H), 4.00 (s, 4H), 4.04 (s, 3H), 4.19 (d, J = 7.8 Hz, 1H), 4.50−4.46 (m, 2H), 4.58 (s, 2H), 6.25 (d, J = 3.9 Hz, 1H), 6.35−6.33 (m, 1H), 6.83 (d, J = 9.3 Hz, 2H), 6.88 (d, J = 4.0 Hz, 1H), 6.99 (d, J = 4.6 Hz, 1H), 7.17 (t, J = 3.9 Hz, 2H), 7.19 (s, 1H), 7.24−7.20 (m, 1H), 7.46 (s, 1H), 7.53 (s, 1H), 7.79 (s, 1H), 7.87 (d, J = 9.2

DOI: 10.1021/ja5106738
J. Am. Chem. Soc. 2015, 137, 1181−1189

Hz, 2H), 8.08 (d, J = 9.1 Hz, 2H), 8.40 (d, J = 9.1 Hz, 2H). ^{13}C NMR (151 MHz, MeOD) δ 175.40, 175.35, 157.88, 155.14, 154.03, 152.37, 150.13, 148.21, 146.05, 145.72, 143.54, 133.43, 132.40, 132.30, 125.96, 125.63, 125.01, 124.82, 121.36, 119.35, 112.84, 112.49, 104.58, 102.39, 101.49, 78.14, 77.02, 75.22, 71.69, 70.95, 68.82, 65.44, 57.45, 52.77, 50.73, 49.72, 49.15, 40.66, 38.91, 37.94, 36.22, 34.11, 33.23, 30.93, 30.47, 25.74, 24.31, 23.88.

In Vitro Kinetic Assays. In vitro GCase assays were conducted on a Cary Eclipse fluorescence spectrophotometer (Varian Inc.). The continuous assay was performed in citrate−phosphate buffer (20 mM, pH 5.5) in the presence of 0.2% taurodeoxycholate at 37 °C. A buffer having a pH of 5.5 was used because GCase shows optimal activity at this pH, which is similar to the pH of lysosomes, the native environment for this enzyme. Additionally, 0.2% taurodeoxycholate was included in these assays because it has been shown this detergent activates this normally membrane-associated enzyme.[46] The concentrations of substrates 4-MUGlc, **9a**, and **9b** used were 1, 2.5, 5, 15, and 20 μM. The final volume of each assay was 160 μL containing 1% dimethyl sulfoxide (DMSO). The reactions were initiated by the addition of recombinant purified GCase (33.5 nM final concentration) for 4-MUGlc and substrate **9a**, whereas GCase (9.3 nM final concentration; R&D Systems) was used for substrate **9b**. The assays were then monitored for 500 s. The instrument excitation and emission wavelengths were set at 338 and 490 nm, respectively, for **9a** with a slit width of 5 nm. The instrument emission filter was set open, excitation filter at auto, and the photomultiplier tube (PMT) voltage at high. The excitation and emission wavelengths were adjusted for substrate **9b** (ex 574 and em 595 nm) and 4-MUGlc (ex 365 and em 450 nm); otherwise all other conditions were the same as described above. Standard curves to quantify 4-MU, EDANS, and BODIPY 576/589 releases were generated under the same conditions as the assays.

Cell Culture. Human primary fibroblast cell lines were cultured, except where indicated otherwise, in α-MEM (without nucleosides) supplemented with 10% fetal bovine serum (FBS) and 1% penicillin−streptomycin at 37 °C and 5% CO_2 at a density of 10 000 cells/mL. The medium was replaced every 3−4 days and the cells were passaged after reaching 70−80% confluency, which occurred approximately every 2 weeks. SK-N-SH (ATCC) cells were cultured in DMEM supplemented with 15% FBS as described above but were seeded in quadruplicate into the central 60 wells of a glass-bottom 96-well plate (Corning 4580).

Live Cell Imaging. Confocal fluorescence microscopy was performed on a Nikon A1R laser scanning confocal system in conjunction with a Nikon Eclipse Ti inverted microscope. All fluorescence images were processed with Volocity quantification software (PerkinElmer). For confocal imaging, fibroblasts were plated on a 35 mm dish with a 1.5 coverglass (MatTek Corp.) in 2 mL of complete growth medium and allowed to grow to 50% confluence. Cells were then washed three times with phosphate-buffered saline (PBS) warmed to 37 °C. A mixture of substrate dissolved in DMSO (0.1% final concentration of DMSO) was added to the imaging medium [0.2× Hank's buffered salt solution (HBSS) containing 0.6% glucose and 40 mM 4-(2-hydroxyethyl)-1-piperazineethanesulfonic acid (HEPES)], which was then added to these cells and incubated at 37 °C and 5% CO_2 in the dark for the times specified. The images were collected by use of a 60× oil objective. The effect of substrate on the viability of cells was assessed by the trypan blue assay (data not shown) after the cells were treated with substrate for 3 and 20 h in imaging medium. The viability of cells was affected by neither the substrate nor the imaging medium.

To assess the effects of cell density on fluorescence per cell, 10 000, 5000, 2500, 1250, 625, and 0 cells were seeded in quadruplicate into the central 60 wells of a glass-bottom 96-well plate (Corning 4580). Cells were allowed to adhere, after which 1 mM CBE (Sigma) was applied to two of the four cultures at each cell density and cells were then cultured for 16 h. The medium from each well was then removed, the cells were washed twice with PBS warmed to 37 °C, and the cells were then fed with MEM containing 5 μM substrate, 1 μM DAPI (Life Technology D3571), and 1% DMSO but lacking phenol red (Gibco 41061-029). After 2 h of incubation, the cells were washed twice with PBS warmed to 37 °C and the cells fed with MEM medium lacking phenol red for imaging on a Cytation 3 cell imaging multi-mode reader (Bio-Tek) with DAPI and Cy3 channels and a 20× objective. Four fields of images were acquired at predefined regions of each well. Data were analyzed by determining the total fluorescence intensity obtained from the Cy3 channel and dividing by the number of cells in an individual field, chosen randomly from two of the fields obtained per well. For the time-course incubation of the substrate, 5000 cells were seeded as described above and allowed to adhere overnight. The experiment was carried out as described above except that 5 μM substrate in DMSO, to yield a 1% final DMSO concentration, was added to duplicate wells at 4, 3, 2, 1, 0.5, 0.12 h prior to imaging. DAPI (1 μM, Life Technology D3571) was added to the wells 2 h before imaging. Imaging and quantification were performed as described above. Dose−response studies were carried out as described above except that duplicate wells contained 1 μM DAPI along with 0, 0.5, 1, 2.5, or 5 μM substrate and 1% DMSO. Cells were incubated for 2 h, and imaging and quantification were performed as described above. SK-N-SH (ATCC) cells were seeded (10 000 cells) in quadruplicate into the central 60 wells of a glass-bottom 96-well plate (Corning 4580). These cells were handled and imaged as described above for human fibroblasts.

Chaperoning Experiments. Primary human fibroblast cells were plated onto 35 mm dishes containing 1.5 coverglass (MatTek Corp.) at 15 000 cells/dish and allowed to adhere overnight. On the second day, growth medium with or without 10 μM inhibitory chaperone AT3375 in 0.1% DMSO final concentration was applied for 5 days. On day 6, the cells were washed with cold PBS three times and then replaced with fresh medium twice 4 h apart. CBE (1 mM) was added in triplicate to control cells cultured in the absence of AT3375 and then allowed to incubate overnight at 37 °C in the presence of 5% CO_2. Finally, the cells were washed with PBS three times and then incubated with substrate **9b** for 3 h, after which the cells were imaged by confocal fluorescence microscopy. Z stacks of images were collected by use of a 40× oil objective. To quantify the activity of the fluorescence substrate, two Z-stack images were acquired from each of three experimental replicates from separate dishes. Two consecutive optical images from the center of the Z stack were converted into 8-bit RGB tiff images for analysis by ImageJ software version 2.30 (NIH, Bethesda, MD). Two regions of interest (ROI) of 4.7 μm × 4.7 μm were defined in the cytosolic space adjacent to the cell nucleus per cell in each image to yield a total of 20 ROI for analysis by densitometry.

Quantitative Immunoblotting. Wild-type human fibroblast cells were cultured as described above in 6-well plates at a density of 0.5 × 10^6 cells/well. Cells were treated with AT3375 at a final concentration of 10 μM for 5 days. Cells were collected and lysed with 1% sodium dodecyl sulfate (SDS), and then 20 μg of protein from each sample was separated by electrophoresis on 4−15% SDS−polyacrylamide minigels (Bio-Rad), transferred to nitrocellulose membrane (Bio-Rad), and immunoblotted with a mouse IgG monoclonal anti-human GCase antibody (R&D Systems) at 1:1000 dilution; rabbit anti-β-actin antibody (LI-COR) was used as a loading control (1:10000 dilution). Protein bands were detected with IRDye 680 conjugated goat anti-mouse IgG and IRDye 800 conjugated goat anti-rabbit secondary antibodies (LI-COR). The blots were scanned using a LI-COR odyssey image system, and densitometry was performed with ImageJ (NIH).

■ ASSOCIATED CONTENT

Supporting Information

Nine figures showing HPLC purification, fluorescence spectra, determination of quenching efficiency, and in vitro GCase assay of substrates **9a** and **9b** and fluorescence data for SK-N-SH cells; NMR spectra for **5**, **6**, **8a**, **8b**, **9a**, and **9b**. This material is available free of charge via the Internet at http://pubs.acs.org.

DOI: 10.1021/ja5106738
J. Am. Chem. Soc. 2015, 137, 1181−1189

AUTHOR INFORMATION

Corresponding Author

*dvocadlo@sfu.ca

Notes

The authors declare the following competing financial interest(s): D.J.V. is a cofounder of and holds equity in the company Alectos Therapeutics. D.J.V. serves as CSO and chair of the Scientific Advisory Board (SAB) of Alectos Therapeutics.

ACKNOWLEDGMENTS

Financial support through a Discovery grant from the Natural Sciences and Engineering Research (NSERC) is gratefully acknowledged. D.J.V. acknowledges the support of the Canada Research Chairs program for a Tier I Canada Research Chair in Chemical Glycobiology and NSERC for support as an E.W.R. Steacie Memorial Fellow. A.R.K. thanks the Michael Smith Foundation for Health Research for a senior scholar award. Alectos Therapeutics is thanked for the gift of AT3375. Michael Tropak and Don Mahuran (Sick Children's Hospital, Toronto) and the Coriell Institute are thanked for providing wild-type human fibroblasts.

REFERENCES

(1) Lombard, V.; Golaconda Ramulu, H.; Drula, E.; Coutinho, P. M.; Henrissat, B. *Nucleic Acids Res.* **2014**, *42*, D490.

(2) Bendikov-Bar, I.; Horowitz, M. *Hum. Mutat.* **2012**, *33*, 1398.

(3) Beutler, E.; Grabowski, G. A. In *The Metabolic and Molecular Bases of Inherited Disease*; Scriver, C. R., Sly, W. S., Childs, B., Valle, D., Childs, B., Kinzler, K., Vogelstein, B., Eds.; McGraw Hill: New York, 2001; p 3635.

(4) Lachmann, R. H.; Grant, I. R.; Halsall, D.; Cox, T. M. *QJM* **2004**, *97*, 199.

(5) Grabowski, G. A. *Lancet* **2008**, *372*, 1263.

(6) Brady, R. O. *Annu. Rev. Med.* **2006**, *57*, 283−296.

(7) Cox, T.; Lachmann, R.; Hollak, C.; Aerts, J.; van Weely, S.; Hrebicek, M.; Platt, F.; Butters, T.; Dwek, R.; Moyses, C.; Gow, I.; Elstein, D.; Zimran, A. *Lancet* **2000**, *355*, 1481.

(8) Fan, J. Q.; Ishii, S.; Asano, N.; Suzuki, Y. *Nat. Med.* **1999**, *5*, 112.

(9) Sawkar, A. R.; Cheng, W. C.; Beutler, E.; Wong, C. H.; Balch, W. E.; Kelly, J. W. *Proc. Natl. Acad. Sci. U.S.A.* **2002**, *99*, 15428.

(10) Neudorfer, O.; Giladi, N.; Elstein, D.; Abrahamov, A.; Turezkite, T.; Aghai, E.; Reches, A.; Bembi, B.; Zimran, A. *QJM* **1996**, *89*, 691.

(11) Wong, K.; Sidransky, E.; Verma, A.; Mixon, T.; Sandberg, G. D.; Wakefield, L. K.; Morrison, A.; Lwin, A.; Colegial, C.; Allman, J. M.; Schiffmann, R. *Mol. Genet. Metab.* **2004**, *82*, 192.

(12) Tayebi, N.; Walker, J.; Stubblefield, B.; Orvisky, E.; LaMarca, M. E.; Wong, K.; Rosenbaum, H.; Schiffmann, R.; Bembi, B.; Sidransky, E. *Mol. Genet. Metab.* **2003**, *79*, 104.

(13) Sidransky, E.; Lopez, G. *Lancet Neurol.* **2012**, *11*, 986.

(14) Nalls, M. A.; Duran, R.; Lopez, G.; Kurzawa-Akanbi, M.; McKeith, I. G.; Chinnery, P. F.; Morris, C. M.; Theuns, J.; Crosiers, D.; Cras, P.; Engelborghs, S.; De Deyn, P. P.; Van Broeckhoven, C.; Mann, D. M.; Snowden, J.; Pickering-Brown, S.; Halliwell, N.; Davidson, Y.; Gibbons, L.; Harris, J.; Sheerin, U. M.; Bras, J.; Hardy, J.; Clark, L.; Marder, K.; Honig, L. S.; Berg, D.; Maetzler, W.; Brockmann, K.; Gasser, T.; Novellino, F.; Quattrone, A.; Annesi, G.; De Marco, E. V.; Rogaeva, E.; Masellis, M.; Black, S. E.; Bilbao, J. M.; Foroud, T.; Ghetti, B.; Nichols, W. C.; Pankratz, N.; Halliday, G.; Lesage, S.; Klebe, S.; Durr, A.; Duyckaerts, C.; Brice, A.; Giasson, B. I.; Trojanowski, J. Q.; Hurtig, H. I.; Tayebi, N.; Landazabal, C.; Knight, M. A.; Keller, M.; Singleton, A. B.; Wolfsberg, T. G.; Sidransky, E. *JAMA Neurol.* **2013**, *70*, 727.

(15) Lwin, A.; Orvisky, E.; Goker-Alpan, O.; LaMarca, M. E.; Sidransky, E. *Mol. Genet. Metab.* **2004**, *81*, 70.

(16) Winder-Rhodes, S. E.; Evans, J. R.; Ban, M.; Mason, S. L.; Williams-Gray, C. H.; Foltynie, T.; Duran, R.; Mencacci, N. E.; Sawcer, S. J.; Barker, R. A. *Brain* **2013**, *136*, 392.

(17) Gegg, M. E.; Burke, D.; Heales, S. J.; Cooper, J. M.; Hardy, J.; Wood, N. W.; Schapira, A. H. *Ann. Neurol.* **2012**, *72*, 455.

(18) Balducci, C.; Pierguidi, L.; Persichetti, E.; Parnetti, L.; Sbaragli, M.; Tassi, C.; Orlacchio, A.; Calabresi, P.; Beccari, T.; Rossi, A. *Mov. Disord.* **2007**, *22*, 1481.

(19) Sardi, S. P.; Clarke, J.; Kinnecom, C.; Tamsett, T. J.; Li, L.; Stanek, L. M.; Passini, M. A.; Grabowski, G. A.; Schlossmacher, M. G.; Sidman, R. L.; Cheng, S. H.; Shihabuddin, L. S. *Proc. Natl. Acad. Sci. U.S.A.* **2011**, *108*, 12101.

(20) Sardi, S. P.; Clarke, J.; Viel, C.; Chan, M.; Tamsett, T. J.; Treleaven, C. M.; Bu, J.; Sweet, L.; Passini, M. A.; Dodge, J. C.; Yu, W. H.; Sidman, R. L.; Cheng, S. H.; Shihabuddin, L. S. *Proc. Natl. Acad. Sci. U.S.A.* **2013**, *110*, 3537.

(21) Richter, F.; Fleming, S. M.; Watson, M.; Lemesre, V.; Pellegrino, L.; Ranes, B.; Zhu, C.; Mortazavi, F.; Mulligan, C. K.; Sioshansi, P. C.; Hean, S.; De La Rosa, K.; Khanna, R.; Flanagan, J.; Lockhart, D. J.; Wustman, B. A.; Clark, S. W.; Chesselet, M. F. *Neurotherapeutics* **2014**, *11*, 840.

(22) Kornhaber, G. J.; Tropak, M. B.; Maegawa, G. H.; Tuske, S. J.; Coales, S. J.; Mahuran, D. J.; Hamuro, Y. *ChemBioChem* **2008**, *9*, 2643.

(23) McNeill, A.; Magalhaes, J.; Shen, C.; Chau, K. Y.; Hughes, D.; Mehta, A.; Foltynie, T.; Cooper, J. M.; Abramov, A. Y.; Gegg, M.; Schapira, A. H. *Brain* **2014**, *137*, 1481.

(24) Tropak, M. B.; Kornhaber, G. J.; Rigat, B. A.; Maegawa, G. H.; Buttner, J. D.; Blanchard, J. E.; Murphy, C.; Tuske, S. J.; Coales, S. J.; Hamuro, Y.; Brown, E. D.; Mahuran, D. J. *ChemBioChem* **2008**, *9*, 2650.

(25) Lorincz, M.; Herzenberg, L. A.; Diwu, Z.; Barranger, J. A.; Kerr, W. G. *Blood* **1997**, *89*, 3412.

(26) Steet, R. A.; Chung, S.; Wustman, B.; Powe, A.; Do, H.; Kornfeld, S. A. *Proc. Natl. Acad. Sci. U.S.A.* **2006**, *103*, 13813.

(27) Witte, M. D.; Kallemeijn, W. W.; Aten, J.; Li, K. Y.; Strijland, A.; Donker-Koopman, W. E.; van den Nieuwendijk, A. M.; Bleijlevens, B.; Kramer, G.; Florea, B. I.; Hooibrink, B.; Hollak, C. E.; Ottenhoff, R.; Boot, R. G.; van der Marel, G. A.; Overkleeft, H. S.; Aerts, J. M. *Nat. Chem. Biol.* **2010**, *6*, 907.

(28) Han, J.; Han, M. S.; Tung, C. H. *Mol. Biosyst.* **2013**, *9*, 3001.

(29) Kamiya, M.; Asanuma, D.; Kuranaga, E.; Takeishi, A.; Sakabe, M.; Miura, M.; Nagano, T.; Urano, Y. *J. Am. Chem. Soc.* **2011**, *133*, 12960.

(30) Redy-Keisar, O.; Kisin-Finfer, E.; Ferber, S.; Satchi-Fainaro, R.; Shabat, D. *Nat. Protoc.* **2014**, *9*, 27.

(31) Debacq-Chainiaux, F.; Erusalimsky, J. D.; Campisi, J.; Toussaint, O. *Nat. Protoc.* **2009**, *4*, 1798.

(32) Edgington, L. E.; Verdoes, M.; Bogyo, M. *Curr. Opin. Chem. Biol.* **2011**, *15*, 798.

(33) Cortez-Retamozo, V.; Swirski, F. K.; Waterman, P.; Yuan, H.; Figueiredo, J. L.; Newton, A. P.; Upadhyay, R.; Vinegoni, C.; Kohler, R.; Blois, J.; Smith, A.; Nahrendorf, M.; Josephson, L.; Weissleder, R.; Pittet, M. J. *J. Clin. Invest.* **2008**, *118*, 4058.

(34) Watzke, A.; Kosec, G.; Kindermann, M.; Jeske, V.; Nestler, H. P.; Turk, V.; Turk, B.; Wendt, K. U. *Angew. Chem., Int. Ed.* **2008**, *47*, 406.

(35) Folk, D. S.; Torosian, J. C.; Hwang, S.; McCafferty, D. G.; Franz, K. J. *Angew. Chem., Int. Ed.* **2012**, *51*, 10795.

(36) Kwan, D. H.; Chen, H. M.; Ratananikom, K.; Hancock, S. M.; Watanabe, Y.; Kongsaeree, P. T.; Samuels, A. L.; Withers, S. G. *Angew. Chem., Int. Ed.* **2011**, *50*, 300.

(37) Komatsu, T.; Kikuchi, K.; Takakusa, H.; Hanaoka, K.; Ueno, T.; Kamiya, M.; Urano, Y.; Nagano, T. *J. Am. Chem. Soc.* **2006**, *128*, 15946.

(38) Joosten, J. A.; Loimaranta, V.; Appeldoorn, C. C.; Haataja, S.; El Maate, F. A.; Liskamp, R. M.; Finne, J.; Pieters, R. J. *J. Med. Chem.* **2004**, *47*, 6499.

(39) Jung, M. E.; Yang, E. C.; Vu, B. T.; Kiankarimi, M.; Spyrou, E.; Kaunitz, J. *J. Med. Chem.* **1999**, *42*, 3899.

DOI: 10.1021/ja5106738
J. Am. Chem. Soc. 2015, 137, 1181−1189

(40) Gnaccarini, C.; Ben-Tahar, W.; Mulani, A.; Roy, I.; Lubell, W. D.; Pelletier, J. N.; Keillor, J. W. *Org. Biomol. Chem.* **2010**, *10*, 5258.
(41) Boot, R. G.; Verhoek, M.; Donker-Koopman, W.; Strijland, A.; van Marle, J.; Overkleeft, H. S.; Wennekes, T.; Aerts, J. M. F. G. *J. Biol. Chem.* **2007**, *282*, 1305.
(42) Hayashi, Y.; Okino, N.; Kakuta, Y.; Shikanai, T.; Tani, M.; Narimatsu, H.; Ito, M. *J. Biol. Chem.* **2007**, *282*, 30889.
(43) Ridley, C. M.; Thur, K. E.; Shanahan, J.; Thillaiappan, N. B.; Shen, A.; Uhl, K.; Walden, C. M.; Rahim, A. A.; Waddington, S. N.; Platt, F. M.; van der Spoel, A. C. *J. Biol. Chem.* **2013**, *288*, 26052.
(44) Kallemeijn, W. W.; Li, K. Y.; Witte, M. D.; Marques, A. R.; Aten, J.; Scheij, S.; Jiang, J.; Willems, L. I.; Voorn-Brouwer, T. M.; van Roomen, C. P.; Ottenhoff, R.; Boot, R. G.; van den Elst, H.; Walvoort, M. T.; Florea, B. I.; Codee, J. D.; van der Marel, G. A.; Aerts, J. M.; Overkleeft, H. S. *Angew. Chem., Int. Ed.* **2012**, *51*, 12529.
(45) Boyd, R.;Lee, G.; Rybczynski, P. (Amicus Therapeutics Inc.) Novel Compositions for Preventing and/or Treating Lysosomal Storage Disorders. U.S. Patent 20140086896, 2014.
(46) Raghavan, S. S.; Topol, J.; Kolodny, E. H. *Am. J. Hum. Genet.* **1980**, *32*, 158.

DOI: 10.1021/ja5106738
J. Am. Chem. Soc. 2015, 137, 1181−1189